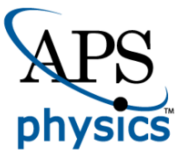



# Ultrafast Switching of Photonic Entanglement

Matthew A. Hall, Joseph B. Altepeter, and Prem Kumar

Phys. Rev. Lett. **106**, 053901 — Published 1 February 2011

DOI: 10.1103/PhysRevLett.106.053901

# Ultrafast switching of photonic entanglement

Matthew A. Hall,[1] Joseph B. Altepeter,[1] and Prem Kumar[1]

[1]*Center for Photonic Communication and Computing, EECS Department*
*Northwestern University, 2145 Sheridan Road, Evanston, IL 60208-3118*

## Abstract

To deploy and operate a quantum network which utilizes existing telecommunications infrastructure, it is necessary to be able to route entangled photons at high speeds, with minimal loss and signal-band noise, and—most importantly—without disturbing the photons' quantum state. Here we present a switch which fulfills these requirements and characterize its performance at the single photon level. Furthermore, because this type of switch couples the temporal and spatial degrees of freedom, it provides an important new tool with which to encode multiple-qubit states in a single photon. As a proof-of-principle demonstration of this capability, we demultiplex a single quantum channel from a dual-channel, time-division-multiplexed entangled photon stream, effectively performing a controlled-bit-flip on a two-qubit subspace of a five-qubit, two-photon state.

PACS numbers:

Next-generation photonic quantum networks will require switches that operate with low loss, low signal-band noise, and *without* disturbing the transmitted photons' spatial, temporal, or polarization degrees of freedom. Additionally, the switch's operational wavelength must be compatible with a low-loss, non-dispersive transmission medium, such as standard optical fiber's 1.3-$\mu$m zero-dispersion band [1, 2]. Unfortunately, no previously demonstrated technology [3]–[14] is capable of *simultaneously* satisfying each of the above requirements: waveguide electro-optic modulators (EOMs) [15] and resonators [16, 17] can operate at very high speeds (10 GHz) but completely destroy any quantum information stored in the polarization degree of freedom; micro-electromechanical switches [5, 18] do not degrade the photon's quantum state, but operate at very low speeds ($<=$ 250 kHz); polarization-independent EOMs [15] can operate at moderate speeds ($\sim$100 MHz) but with relatively high loss; and finally, traditional 1550-nm devices based on nonlinear-optical fiber loops [6, 19] generate unacceptably high levels of Raman-induced noise ($>$ 1 in-band noise photon per 100-ps switching window [20]).

Although the requirements for ultrafast entangled-photon switching are collectively daunting, they describe a device that is capable of selectively coupling the spatial and temporal degrees of photonic quantum information. In other words, a device that can encode multiple-qubit quantum states onto a single photon, enabling quantum communication protocols that exploit high-dimensional spatio-temporal encodings. In this Letter we describe the construction and characterization of an all-optical switch which meets each of the aforementioned requirements, and whose aggregate performance (in terms of loss, speed, and in-band noise) exceeds that of all available alternatives [3]–[19]. Moreover, this switch design is scalable: by its extension one can create devices that are capable of coupling many temporal qubits and many spatial qubits. As a proof-of-principle demonstration of this capability, we utilize the switch to perform a controlled-bit-flip operation on a two-qubit subspace of a two-photon, five-qubit system, where a temporally encoded qubit is used as the control and a spatially encoded qubit is used as the target. This operation is used to demultiplex a single quantum channel from a dual-channel, time-division-multiplexed entangled photon stream encoded into the larger five-qubit space.

To simultaneously achieve low loss and ultrafast switching, we utilize an all-optical, fiber-based design in which bright 1550-nm pump (C-band) pulses control the trajectory of 1310-nm (O-band) single-photon signals (see Fig. 1(b)). Physically, this switch exploits

polarization-insensitive cross-phase modulation (XPM) [21] in a nonlinear-optical loop mirror (NOLM) [22], the reflectivity of which is determined by the phase difference between the clockwise and counter-clockwise propagating paths in a fiber Sagnac interferometer (the "loop") [23]. To actively control the state of this switch, we initially configure an intra-loop fiber polarization controller such that the loop *reflects* all incoming photons. Multiplexing a strong 1550-nm pump pulse into the clockwise loop path then creates an XPM-induced phase shift on the clockwise signal amplitude, with a $\pi$ phase shift causing the switch to *transmit all* incoming photons. As XPM is polarization dependent, it is important that the pump is effectively unpolarized. We accomplish this by temporally overlapping two orthogonally polarized pump pulses, each with a slightly different wavelength [21].

Note that the traditional NOLM-based C-band devices are unsuitible for single-photon switching for two reasons: Firstly, and most importantly, such switches generate very high levels of Raman-induced background photons at signal wavelenths [20]. These noise photons would swamp any single-photon signals, effectively "washing out" any two-photon quantum correlations. Secondly, traditional NOLM-based devices utilize pump pulses which are group-velocity matched to the signals being switched. While this increases the interaction time, the nonlinear character of the XPM process limits the switching contrast in this type of operation. Because the pump pulse can not be made perfectly square-shaped, the center of the signal pulse receives a stronger nonlinear phase shift than the pulse wings, making it effectively impossible to choose a single pump power which maximizes switching contrast over the entire signal pulse.

Our switch design is immune to each of these two fundamental problems and allows for noiseless, high contrast switching operation. Firstly, the large anti-Stokes detuning ($\approx$35 THz) between the 1550-nm pump pulses and the 1310-nm single-photon pulses reduces contamination of the quantum channels by spontaneous Raman scattering of the pump ($\approx 2 \times 10^{-7}$ background photons per ps of signal pulse). Secondly, in standard single-mode fiber (the loop medium) this detuning leads to a large group-velocity difference ($\approx$2 ps/m) between the pump and signal pulses. This allows the switch to operate in a regime where the pump pulse walks completely through the signal's temporal mode, providing the type of uniform phase-shift which is essential for high-contrast switching operation. The effective phase shift is therefore determined by the total energy in a single pump pulse, regardless of that pulse's temporal profile. The switching *window*, $\tau$, is in turn determined by the *length*

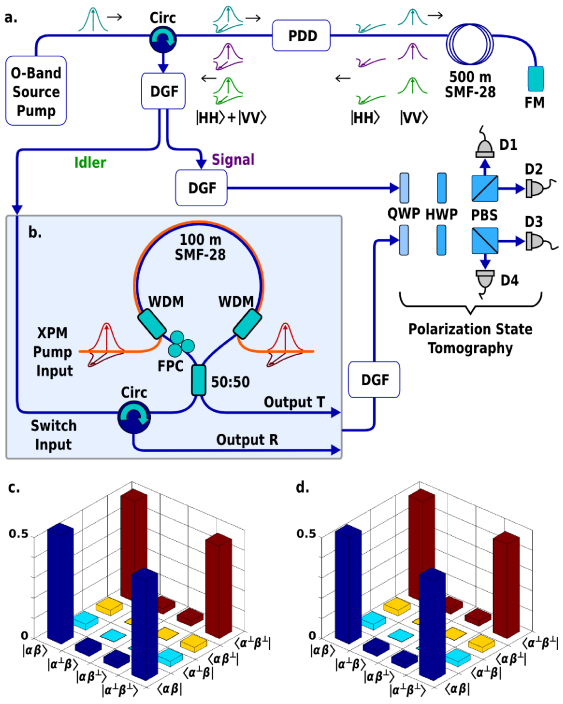


FIG. 1: (a) Entangled photon-pair source and switching test apparatus. Nondegenerate pairs ($\lambda_{\text{signal}} = 1303.5$ nm and $\lambda_{\text{idler}} = 1306.5$ nm) are generated in 500 m of standard single-mode fiber (SMF-28) and separated using a double-pass grating filter (DGF). Circ: circulator, FM: Faraday mirror, FPC: fiber polarization controller, HWP/QWP: half/quarter-wave plate, PBS: polarizing beam-splitter, PDD: polarization dependent delay, WDM: wavelength-division multiplexer. (b) The single-photon switch. The length of the intra-loop SMF-28 is directly proportional to the switching window. An $L_{100} \equiv$ 100-m loop (shown) results in a ≈200-ps switching window. (c) Reconstructed density matrix of the unswitched state for $L_{100}$ (fidelity to a maximally entangled state, $F = 99.5\% \pm 0.2\%$). (d) Density matrix of the switched state for $L_{100}$ ($F = 99.4\% \pm 0.4\%$). Similar reconstructions for the 500-m switch (not shown) yielded $F = 99.5\% \pm 0.2\%$ (unswitched) and $F = 99.2\% \pm 0.2\%$ (switched).

*of the fiber* between the WDMs, $L$, multiplied by the speed at which the signal sweeps through the pump (i.e., the group velocity difference between signal and pump). For our case, $\tau = L \times 2$ ps/m. The turn-on time is set by the temporal extent of the pump pulses (i.e., the time it takes for the pump to physically enter the fiber loop). For 5-nm bandwidth, transform-limited C-band pump pulses, for example, the turn-on time can be as short as 1 ps.

Two key experimental technologies are required to operate and characterize this type of

switch: a short-pulse dual-wavelength 1550-nm pump and a source of 1310-nm entangled photons. To create the dual-wavelength pump, two 5-ps duration pulses (1545-nm and 1555-nm) are spectrally carved from the output of a 50-MHz repetition rate mode-locked fiber laser (IMRA Femtolite Ultra) and multiplexed using a polarization beam combiner. The power necessary to produce a $\pi$ phase shift is obtained using a cascade of erbium-doped fiber amplifiers (EDFAs). A long-pass filter after each EDFA ensures that no contaminating O-band photons are introduced.

The IMRA laser also provides an electrical clock signal for a 1310-nm entangled photon source and an array of four single-photon detectors. The entangled photon source, described in detail in reference [2] and shown in Fig. 1(a), utilizes spontaneous four-wave-mixing in standard single-mode fiber to produce pairs of polarization-entangled photons from 100-ps wide, 50-MHz repetition-rate pump pulses at 1305 nm. After switching, the photon pairs are measured with a correlated photon detection system (Nucrypt CPDS-4) consisting of an array of four InGaAs/InP avalanche photodiodes.

To test the switch's effectiveness for quantum communications, we measured active and passive switching of polarization-entangled photon pairs. Fig. 1(b) shows the switch integrated into entangled photon source referenced above. To test multiple switching windows, loop lengths of $L_{500} \equiv 500$ m ($\approx$900-ps window) and $L_{100} \equiv 100$ m ($\approx$180-ps window) were used. The insertion loss introducecd by these switches in the O-band quantum channel was measured to be 1.3 dB ($L_{100}$, port T), 1.7 dB ($L_{100}$, port R), 1.7 dB ($L_{500}$, port T), and 2.1 dB ($L_{500}$, port R). Because all of these directly measured losses include the 0.4 dB or 0.8 dB loss from one or two passes through an optical circulator, the raw switching loss for either transmission through or reflection from the switch is 0.9 dB (1.3 dB) for the $L_{100}$ ($L_{500}$) loop.

To set a performance benchmark for the switch, unswitched (no pump) entangled photons from port R were characterized using coincidence-basis quantum-state tomography [24, 25]. Both signal and idler photons were analyzed using separate quarter waveplate, half waveplate, polarizing beam splitter combinations, which together perform arbitrary single qubit measurements. The measured coincidence rates—after subtracting accidental coincidences, a procedure which lowers statistical errors [26]—for 36 combinations of analyzer settings [27] were subjected to a numerical maximum likelihood optimization, which reconstructs the density matrix most likely to have produced the measured results. Figs. 1(c) and

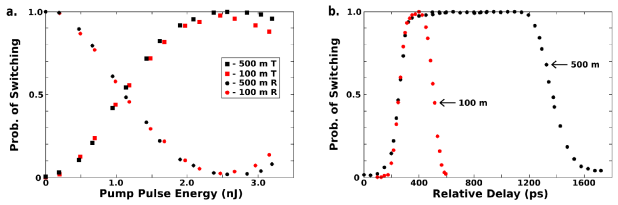


FIG. 2: (a) Single-photon switching contrast. Plot shows switching probability versus pump energy for $L_{500}$ and $L_{100}$ (detector dark counts subtracted). (b) Temporal extent of the switching window, as measured using single photons. Plot shows single-photon counts versus relative delay between the single-photon and the pump pulses (dark counts subtracted).

1(d), respectively, show reconstructed density matrices for passively switched (port R) and actively switched (port T) entangled photons, after reflection or transmission through the $L_{100}$ loop. Similar reconstructions were performed for the $L_{500}$ loop; in all four cases, the fidelity of the measured state to a maximally-entangled state exceeded 99.0%. In addition, no measureable state degradation resulted from active versus passive switching.

Another important metric for both quantum and classical routers is the switching *contrast*—or the ratio of power directed to the desired output port divided by the power directed to the complementary output port. Fig. 2(a) shows the single-photon switching contrast as a function of the pump-pulse energy. A contrast of 120:1 is achieved at a pump energy of 2.5 nJ for $L_{500}$. Although the switching contrast is expected to be independent of $L$, the 100-m data does not appear to achieve full contrast—only 43:1. This artifact is due to a long, low-power tail (≈370-ps total pulse width) in the 1305-nm pump pulses that drive the entangled photon source. Although the entangled photon production rate is proportional to the pump-power *squared*, this still results in a longer than 200-ps pulse width for the entangled photons used to test the switch. As a result, the switching window is too short to completely envelop the photon to be switched, resulting in an artifically lower switching contrast for the $L_{100}$ loop. We expect the true switching contrast to be the same in both cases ($\geq$ 120:1).

Closely related to contrast is the generated single-photon background, from—for example—Raman scattering of the 1550-nm pump pulses. We measured the probability of generating a 1310-nm background photon count and found it to be proportional to $L$ ($\approx 4 \times 10^{-7}\mathrm{m}^{-1}$).

In addition to its use as a single-photon router, the switch is a spatio-temporal coupler,

enabling the encoding and decoding of quantum information into a temporally multimode Hilbert space, which is, in principle, boundless. The extent to which this Hilbert space can be effectively accessed, however, is determined by the temporal switching profiles of the devices described above. To characterize the shape and width of the switching window, we introduce a relative delay between the signal and the pump pulses. Sweeping this delay while measuring the switched single photons we map the switching window (shown in Fig. 2(b)). Note that the temporal extent of the photons being switched blurs the true switching window. To quantitatively estimate the extent of this blurring, we directly measure the temporal shape of the 1305-nm pump pulses used to create the test photons. We perform this measurement by constructing a third $L = 2$-m switch with a switching window of ≈10-ps. Using the now-characterized 1305-nm pump pulses, we re-measure the switching windows while applying a numerical-fit deconvolution to the results, obtaining the instantaneous temporal widths of the 100-m and 500-m switching windows to be 180 ps and 900 ps, respectively.

The switch's ability to manipulate spatial and temporal quantum information has the potential to enable new quantum communication protocols. As an example of this functionality, we use the switch to demultiplex a single quantum channel from a dual-channel entangled photon stream, on which we encode a five-qubit space (see Fig. 3(a)) defined by signal and idler polarization qubits ($|H^{s,i}\rangle, |V^{s,i}\rangle$), signal and idler temporal qubits ($|t_0^{s,i}\rangle, |t_1^{s,i}\rangle$), and an idler spatial qubit ($|T^i\rangle, |R^i\rangle$—see Fig. 1(b)). Using this encoding, we create the five-qubit hyper-entangled state $|\Phi\rangle = c_1|\psi_1\rangle|t_0^s\rangle|t_0^i\rangle|T^i\rangle + c_2|\psi_2\rangle|t_1^s\rangle|t_1^i\rangle|T^i\rangle$, where $|\psi_1\rangle \equiv \frac{1}{\sqrt{2}}(|H^s\rangle|H^i\rangle + |V^s\rangle|V^i\rangle)$, $|\psi_2\rangle \equiv \frac{1}{\sqrt{2}}(|H^s\rangle|H^i\rangle - |V^s\rangle|V^i\rangle)$, and $c_1$ and $c_2$ are arbitrary coefficients. Measuring $|\Phi\rangle$ using polarization-basis tomography while *tracing out* temporal degrees of freedom and *projecting* into the idler spatial mode $|T^i\rangle$ will yield a highly mixed state, exactly the result one expects from a simultaneous measurement of multiple entangled quantum channels. A switch capable of implementing a controlled-NOT operation which couples the spatial and temporal qubits (see Fig. 3(a)), however, would transform $|\Phi\rangle$ into the state: $|\Phi'\rangle = c_1|\psi_1\rangle|t_0^s\rangle|t_0^i\rangle|T^i\rangle + c_2|\psi_2\rangle|t_1^s\rangle|t_1^i\rangle|R^i\rangle$. This demultiplexed state should exhibit maximal entanglement when *projected* into the spatial mode $|T^i\rangle$, because even after tracing over the temporal degrees of freedom only the maximally entangled polarization state $|\psi_1\rangle$ would be present.

To implement this proof-of-principle test of the switch's ability to couple spatial and temporal degrees of freedom, we modify our O-band entangled-photon source [2] by pumping

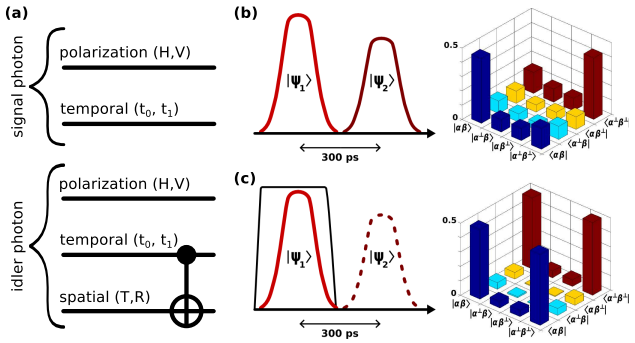


FIG. 3: (a) Diagram of the five degrees of freedom in a multiplexed entangled photon stream, which can be demultiplexed by applying the controlled switch operation (shown). (b) Arrangement of detected quantum information channels for the five-qubit state $|\Phi\rangle$. Tracing over the temporal qubit and projecting into spatial mode $|T^i\rangle$, we reconstruct a highly mixed density matrix with $F = 58.9\% \pm 0.5\%$. (c) Arrangement of quantum information channels after active switching to output T (i.e., demultiplexing), which should produce the state $|\Phi'\rangle$. By projecting into spatial mode $|T^i\rangle$ we recover the maximally entangled state $|\psi_1\rangle$ ($F = 98.6\% \pm 0.7\%$).

it with a pair of pulses separated by $\Delta t \equiv t_1 - t_0 \approx 300$ps. The polarizations of the leading and trailing pump pulses are chosen such that the unnormalized pump state is $\sqrt{c_1}\,(|H^p\rangle + |V^p\rangle)\,t_0 + \sqrt{c_2}\,(|H^p\rangle + i|V^p\rangle)\,t_1$ which upon SFWM gives the output signal-idler state $|\Phi\rangle$. For the demultiplexing test, we choose $c_1/c_2 \approx 1.25$ and $\Delta t \approx 300$ ps.

Figure 3(b) shows the measured density matrix for the multiplexed quantum channels. As expected, the state is highly mixed; its fidelity to the nearest maximally entangled state is only 58.9%. Utilizing the 100-m switch we then demultiplex (i.e., actively switch) only the first quantum channel ($t = t_0$), creating the state $|\Phi'\rangle$. As shown in Fig. 3(d), after demultiplexing we are able to recover the high fidelity (98.6%) of the target state to a maximally entangled state. Because the cross-Kerr phase shift has previously been shown to maintain spatial and temporal coherence in NOLM switches [6, 19], we anticipate that this switch's cross-Kerr-based demultiplexing operation is in fact coherent and equivalent to the controlled-NOT operation depicted in Fig. 3(a). Moreover, unlike LOQC-based gates, this switch is completely deterministic and easily extensible, capable of independently tunable couplings (e.g., controlled-$\pi/4$) to many temporal qubits encoded onto the same photon (by changing the control-pulse's intensity as a function of time). By cascading several switches, it is also possible to couple to multiple spatial qubits.

In conclusion, we have demonstrated the first all-optical switch suitable for single-photon quantum communications. It achieves low-loss, high-isolation, and high-speed, performance without disturbing the quantum state of the routed single photons. Very few fundamental limitations apply to this type of switch design. With carefully designed fiber components, one has the potential to dramatically reduce the switch's loss. In principle the only unavoidable switching losses are fiber transmission losses (0.15–0.2 dB/km) and circulator insertion losses (waveguide-based circulators with a 0.05 dB insertion loss have been designed and simulated [28]). Additionally, decreasing $L$ to a few meters will reduce the switch's speed to $\approx$10 ps while simultaneously decreasing the background by an order of magnitude. Even without these improvements, however, this switch represents an important new tool for manipulating spatially- and temporally-encoded quantum information.

This research was supported in part by the DARPA ZOE program (Grant No. W31P4Q-09-1-0014) and the NSF IGERT Fellowship (Grant No. DGE-0801685).

[1] N. I. Nweke, *et al. Appl. Phys. Lett.* **87**, 174103 (2005).

[2] M. A. Hall, J. B. Altepeter, and P. Kumar, *Optics Express* **17**, 14558 (2009).

[3] M. A. Duguay and J. W. Hansen, *Appl. Phys. Lett.* **15**, 192 (1969).

[4] N. J. Doran and D. Wood, *Opt. Lett.* **13**, 56–58 (1988).

[5] K. Hogari and T. Matsumoto, *Appl. Opt.* **30**, 1253–1257 (1991).

[6] M. Eiselt, *Electron Lett.* **28**, 1505 (1992).

[7] J. P. Sokoloff, P. R. Prucnal, I. Glesk, M. Kane, *IEEE Photon. Technol. Lett.* **5**, 787 (1993).

[8] M. Asobe, I. Yokohama, H. Itoh, and T. Kaino, *Opt. Lett.* **22**, 274 (1997).

[9] I. Yokohama *et al.*, *J. Opt. Soc. Am. B* **14**, 3368 (1997).

[10] G. S. Kanter, P. Kumar, K. R. Parameswaran, and M. M. Fejer, *IEEE Photon. Technol. Lett.* **13**, 341 (2001).

[11] J. E. Sharping, M. Fiorentino, P. Kumar, and R. S. Windeler, *IEEE Photon. Technol. Lett.* **14**, 77 (2002).

[12] V. Van, *et al. IEEE Photon. Technol. Lett.* **14**, 74 (2002).

[13] V. R. Almeida, *et al. Opt. Lett.* **29**, 2867 (2004).

[14] G. Bertocchi, *et al. J. Phys. B* **39** 1011 (2006).

[15] http://www.eospace.com

[16] V. R. Almeida *et al.*, *Opt. Lett.* **29**, 2867–2869 (2004).

[17] P. Dong, S. F. Preble, and M. Lipson, *Opt. Express* **15**, 9600–9605 (2007).

[18] C. Knoernschild, C. Kim, F. P. Lu, and J. Kim, *Opt. Express* **17**, 7233–7244 (2009).

[19] K. Uchiyama *et al.*, *J. Lightw. Tech.* **15**, 194–201 (1997).

[20] Q. Lin, F. Yaman, and G. P. Agrawal, *Phys. Rev. A* **75**, 023803 (2007).

[21] H. Bülow and G. Veith, *Elect. Lett.* **29**, 588–589 (1993). If one pump leads the other by $\delta$, then the leading/trailing $\delta$ parts of the window will be polarization-dependent.

[22] K. J. Blow, N. J. Doran, B. K. Nayar, and B. P. Nelson, *Opt. Lett.* **15**, 248–250 (1990).

[23] D. Mortimer, *J. Lightw. Tech.* **6**, 1217–12124 (1989).

[24] D. F. V. James, P. G. Kwiat, W. J. Munro, and A. G. White, *Phys. Rev. A* **64**, 052312 (2001).

[25] J. B. Altepeter, E. R. Jeffrey, and P. G. Kwiat, *Advances in AMO Physics, Vol. 52*, Ch. 3 (Elsevier, 2006).

[26] Increasing this source's pair production rate (PPR) and subtracting accidental coincidences increases measurement precision while accurately predicting the low-PPR, non-accidental subtracted result [2]. Without this correction, high-PPR, dark-count-only subtracted fidelities for the data in Figs. 1 and 3 are between 80–95%.

[27] J. B. Altepeter, *et al. Phys. Rev. Lett.* **95**, 033601 (2005).

[28] R. Takei and T. Mizumoto, *Jpn. J. Appl. Phys.* **49**, 052203 (2010).